LEGIBILITY NOTICE

A major purpose of the Technical Information Center is to provide the broadest dissemination possible of information contained in DOE's Research and Development Reports to business, industry, the academic community, and federal, state and local governments.

Although a small portion of this report is not reproducible, it is being made available to expedite the availability of information on the research discussed herein.

LA-UR--90-1848

DE90 012155

CHIP BREAKING AND CONTROL FOR A PRECISION AUTOMATED TURNING SYSTEM

Marvin W. Burnham, Ph.D.
The BDM Corporation

Leonard A. Abbatiello
Martin Marietta Energy Systems

Advanced Machining Technology III Conference

CHIP BREAKING AND CONTROL FOR A PRECISION AUTOMATED TURNING SYSTEM

Marvin W. Burnham, Ph.D.

Leonard A. Abbatiello

ABSTRACT

Chip breaking and control is essential to automatic operation of precision turning systems. Failure to transfer parts and system jams can occur if chip fragments are not continuously removed. Surface damage and tool breakage also result from chips that are permitted to wrap around the tool. Also, with increasing environmental concerns, chip handling and recycling are becoming major issues in manufacturing. New information on a variety of mechanisms for breaking chips and methods for removal from the system are discussed. Some of the chip breaking methods are evaluated for the range of cutting in which they are effective. Chip curl and chip breaking analyzed carefully by Nakayama and others is expanded to more fully understand the ways in which chips can be broken.

INTRODUCTION

The recent trend toward unmanned or remote manned manufacturing systems requires automated chip control. Without reliable chip breaking, parts can fail to transfer, tools may be damaged, and the workpiece can be damaged. It is futile to automate all operations and still require an operator to pull out tangled chips with tweezers. In the past few years, concern has increased for the environment and for safety and health issues. As a result, the chips are no longer being thought of as waste but rather as a product. Product status demands concerns for configuration and all phases of handling and packaging. It is likely that in a few years, all pieces of unusable stock as well as chips from machining will be recycled. Chip recovery will be a must.

Most of the available methods of chip breaking have been analyzed in a recent effort to produce an automated, unmanned, accurate turning system[1]. These methods include conventional mechanical chip breakers, hydraulic jet assisted breaking, interruption by precut grooves, interruption using programmed withdrawal of the tool, and capture methods. Most of the methods require a better basis for understanding the chip and its formation. A finite element study is in process to combine the thermal as well as mechanical aspects of chip formation. At the present time, the finite element method is limited to two dimensional chip formation. However, an understanding is needed of the basic physical principals determining the geometry of the chip to be broken. This paper reports a study examining the cross sectional shape of the chip and some implications to chip breaking. Many of the methods require a controlled chip flow direction, chip cross section, and curl form. This analysis provides a basis for these requirements.

Recent studies[1] showed that it was six to ten times easier to break chips in the transverse direction rather than with deflections normal to the tool face. That raised an interesting question: "Are we

deforming chips in the best direction to break them?" Abbatiello found confirmation of the observation by an approximate analysis done by Massa* of Kennametal. Further study reported here focuses on the relation between Colwell's[2] cutting edge chord (CEC) model and the chip cross sectional shape. The theoretical shape then permits a look at the easiest way to break chips at or near the root.

This analysis based on cutting at the tool tip is shown to agree very well with micrographs of chip cross sections from several metals with various degrees of work hardening. Then the implications of the results are discussed in relation to chip breaker design and cutting strategies needed for chip breaking. Many papers have listed product integrity reasons which urge good chip breaking[1,3-6]. Chip jams to an automated system require chip breaking for true automation[1,7,8,10].

With all the urgency to good reliable chip breaking, there is a major opposed concern. That is, the primary goal of machining is to make quality machined components. Product quality must be the driving issue in selecting depths of cut, feed rates, tool nose radii, cutting speeds and other cutting variables. In addition, the economics of the time needed to make parts plays a role in the selection of machining variables. Conventional strategies of moving from unbroken chip regions into conditions leading to broken chips depend on placing depth of cut, feed, and tool nose radius choices under the control of chip breaking. The ruling criterion cannot be both ways, either it is quality and economics or it is chip breaking which selects depths of cut, feed, and nose radius. In addition, the depth of cut varies because there is a tolerance to the contour of the machining blanks. We must understand the physical basis of chip breaking if we hope to break chips without such restrictions. An interesting by product of the analysis is that the result can be beneficial to ultraprecision machining such as diamond turning.

UNDERSTANDING THE CHIP CROSS SECTION

A detailed derivation will be given in Appendix 1. Enough information is given here to understand the approach and method of analysis.

The brief description of the formation of the chip cross section is that a curved boundary caused by the round tool nose radius meets a plane tool rake face and is deformed to the plane shape. The top part of the chip cross section (opposed to the rake face boundary) is formed by the intersection of the groove from the previous tool passage and the uncut workpiece represented by the feed. This is illustrated in Figure 1 (on the next page) that includes a curved shear surface from the curved tool tip up to the approaching workpiece surface. The basis for the analysis is shown in the familiar orthogonal cutting model and the cutting edge chord[11] representation of a curved tool tip shown in Figure 2.

In the text to follow, the notation shown in the figures will be used. Notice that the shear angle is ϕ, the rake angle is α, the cut depth is D_c on the orthogonal model and D on the curved tool nose

* Massa, T.R. "Theoretical Model of the Chipbreaking Process", Kennametal, Private communication, Dec. 1988

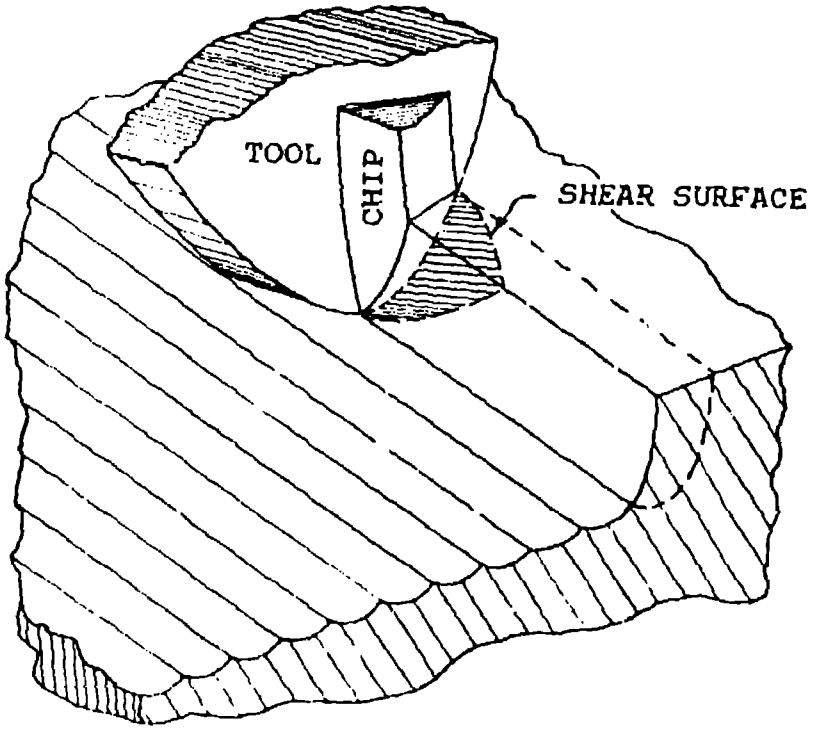

Figure 1 Tool Tip Chip Formation

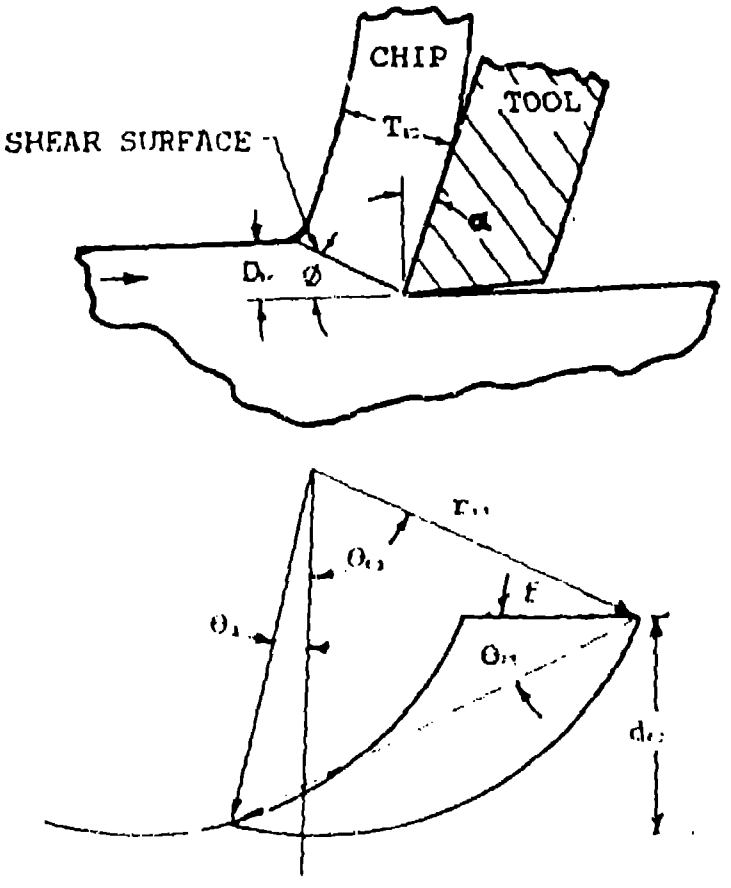

Figure 2 Cutting Notation

radius to represent the usual understanding of the term. The feed is F.

Using the concepts illustrated, the basis for the shape of the chip cross section can now be shown in Figure 3. Notice that in the top illustration, the cross section of the cut has an approximate crescent shaped footprint as seen by the tool face. The added deformation from the current tool edge curve to the cutting edge chord is that amount needed to make the curved surface conform to the tool rake face. Thus, that amount of material may be considered to be added to the top chip contour as in the bottom illustration. The flow direction normal to the CEC is well established experimentally[3-8].

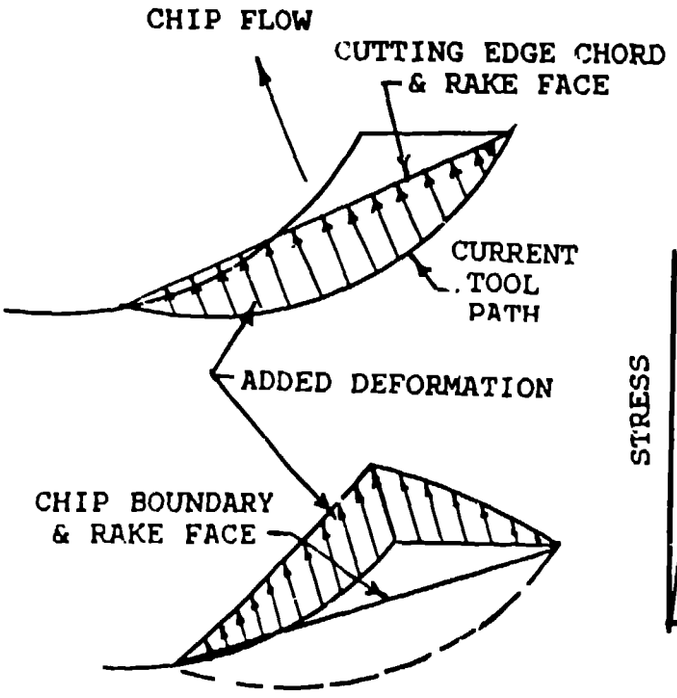

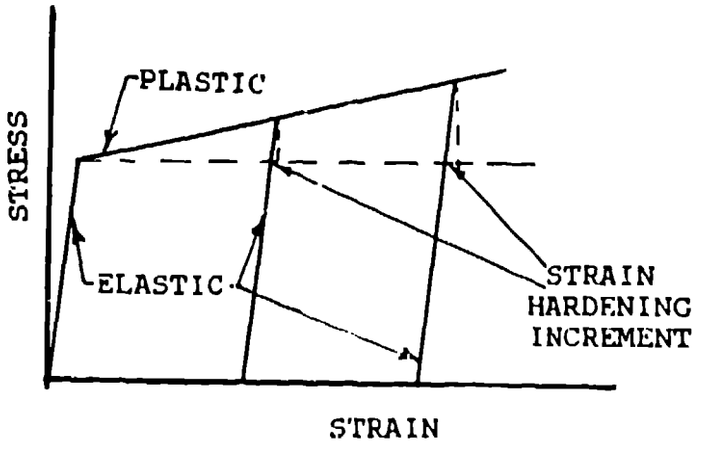

Figure 3 Forming a Chip Cross Section

Figure 4 Strain Hardening

The general process described above assumes (a) that there is no difference in elastic recovery from one element to the next along the CEC, and (b) that the same shear angle applies to all elements. In some materials there is work hardening which causes the elastic recovery to depend on the amount of strain each element experiences. The elastic recovery or spring back then depends on the relative strain from one element to another and the work hardening characteristics. The relative strain was illustrated in the added deformation shown on Figure 3. If the shear angle is the same for all elements, then the boundary for a chip with spring back would be a circular curve of larger radius than the tool nose. The radius of the spring back boundary would depend on the slope of the plastic portion of the stress strain diagram shown in Figure 4. Notice that if the material were ideally plastic (slope of zero) there would be no spring back. The slope of the plastic portion and the total strain determine the amount of spring back so materials that work harden produce spring back proportionate to their material properties.

Although few materials have a linear strain hardening behavior, the observation concerning the slope of the plastic strain curve apply. This will provide a basis for understanding the results. The shear angle assumption will be validated by the results.

The spring back boundary is only approximately circular because of the nonlinear plastic characteristics and because the shear plane is not exactly normal to the tool rake face. Also, if the coolant is not effective, the small chip can partially anneal causing some curvature change. These apparently are immeasurably small influences on the chip cross section as will be seen.

The elements near the ends of the CEC in Figures 2 and 3 have zero uncut chip thickness (distance between surfaces normal to the CEC) while those near the midpoint have large thickness. This means the total strain near the ends is small so that those regions should be softer after the chip is formed.

COMPARISON WITH CHIP CROSS SECTION MICROGRAPHS

Several micrographs from different cutting conditions and using metals with differing strain hardening characteristics are now compared with the cross section analysis. These include some stainless steels and materials like various steels. This will test the predictive capability of the model described. The computer generated boundaries superimposed on the micrograph enlargements were calculated using the equations derived in Appendix I.

Figures 5-7 (next page) show plots of chips made by cutting a hemisphere with a 0.030 inch tool nose radius at 0.005 inch depth of cut and 0.003 inch/revolution feed. The metal has a small strain hardening slope, at least for the range of strains in the cuts made. A tracing of an actual chip cross section micrograph is superimposed. Figure 5 was a cut at the pole of the hemisphere, Figure 6 was at a position 0.25 inches from the pole, and Figure 7 was near the equator. In the equator region the 8 inch O.C. hemisphere has 300 sfm cutting speed. The surface speed(sfm) was constant until the cut reached a position about 1 inch from the pole, at which point the rpm was held constant during cutting to the pole. Thus, in the last inch, the cutting speed linearly declines with decreased radius from the pole. Notice the small curvature of the bottom boundary shows only a small amount of spring back. Also, the bent edges on some chips show a lack of work hardening at the chip edges.

Figures 8-10 show a similar test of the predictive ability of the theory. This material has a much greater slope to the strain hardening curve. As a result, there is more curvature to the lower boundary of the cross section. Also, observe how well the circle (constant radius) agrees with the micrograph. This verifies the assumption that the same shear angle applies to all elements of the uncut chip cross section. Estimates of the error by assuming a constant shear angle are apparently less than 2%. These chip cross sections follow the same sequence in position on the hemisphere as that in the first three figures. The only difference is a greater strain hardening rate material and a feed of 0.0075 inch/revolution. It may be noted in

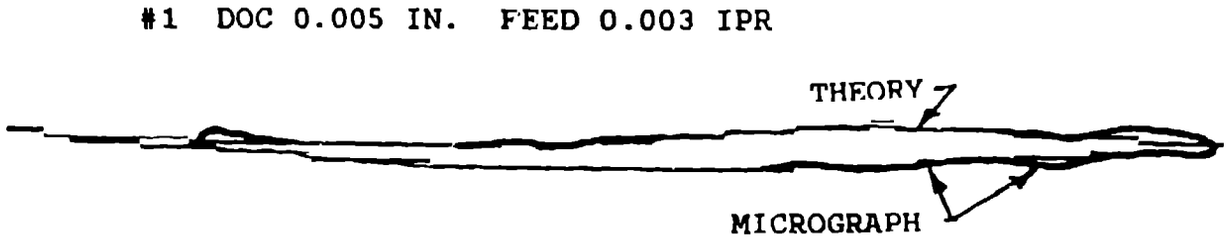

Figure 5 At the Pole - Small Strain Hardening

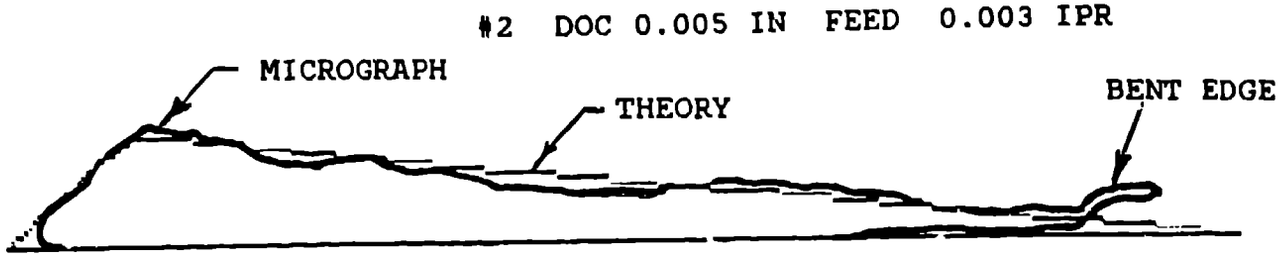

Figure 6 Near the Pole (1/4 in.) Small Strain Hardening

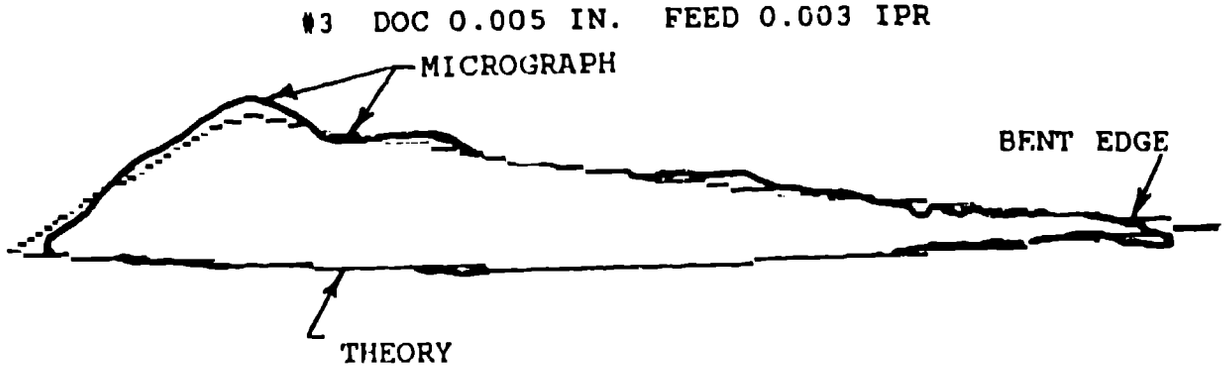

Figure 7 At the Equator - Small Strain Hardening

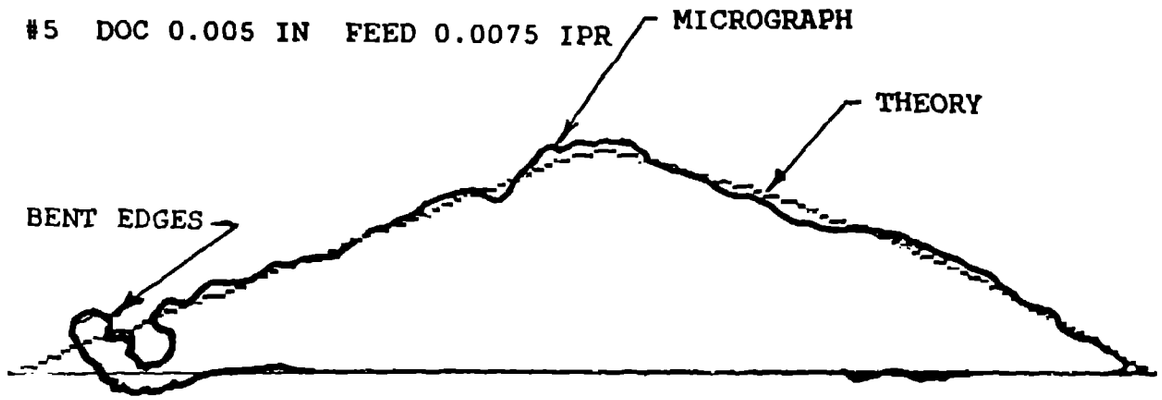

Figure 8 At the Pole - Strong Strain Hardening

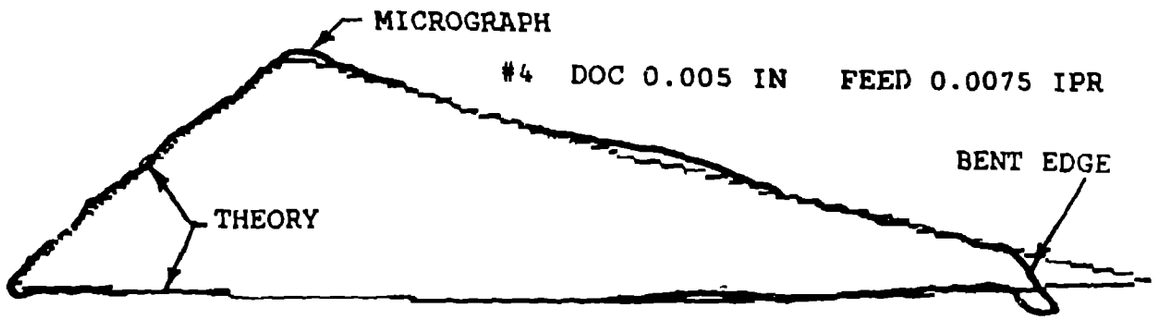

Figure 9 Near the Pole (1/4 in.) Strong Strain Hardening

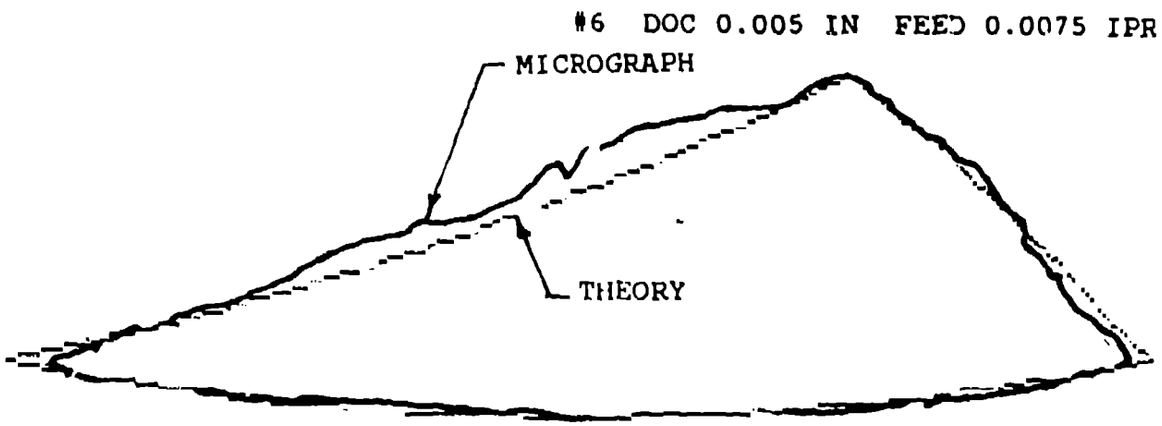

Figure 10 At the Equator - Strong Strain Hardening

the previous micrographs that some of the edges were bent without breaking which verifies the relatively soft condition there.

Figures 11-12 show a material with about the same or lower strain hardening rate as that in Figures 5-7. Figure 11 was cut at a depth of cut of 0.002 inch and Figure 12 was at 0.010 inch. Both were cut with a 0.002 inch/revolution feed and a speed of 300 sfm. Again there is good agreement, although one vertex appears to have been broken off either in cutting or in making the micrograph for Figure 12. Since the outer part of the chip surface is rough, small variations would be expected if several micrographs were made at successive locations on the same chip.

These comparisons appear to verify the analysis, and now some implications for chip breaking and chip breaking operational strategies will be examined.

CHANGES IN CROSS SECTION WITH FEED AND DEPTH OF CUT

Comparison with actual chip geometries is sufficiently good to warrant examination of what happens to the cross section when machining variables change. In all these cases, the feed, depth of cut, and the dimensions of the cross section have been normalized by dividing by the tool nose radius. Although the experiments used a 0.030 inch tool nose radius, the results can apply to any tool nose radius by multiplying by the actual radius. Figure 13 shows the changes in shape when the depth of cut is constant and the feed is varied. Several depths of cut are shown in successive plots. These were all done with no spring back or for materials that behave in nearly an ideally plastic manner in machining. Notice that the thickness vertex varies both in height and in position. Therefore, the centroid and the ideal position to apply a load to bend the chip change. This change is true whether breaking occurs by failure stress near the chip root or by decreasing the chip curl radius so that contact with the tool or the workpiece might break it. The normalized values for feed and depth of cut were chosen to make it easy to relate them to actual values using a 0.030 inch radius tool.

Using a constant feed and varying the depth of cut, the geometry changes as in Figure 14. Once again, both the magnitude and location of the chip thickness vertex changes.

The usual experimental plot of the conditions leading to broken chips is shown in Figure 15. Notice that the strategies usually involve increasing feed if operating in example A, increasing depth of cut if operating at B, and increasing both feed and depth of cut if operating at C. None of these strategies recognize the shift in centroid (neutral axis) location or the position of the shear center. Therefore, the mode of chip breaking is likely to change because the chip geometry changes.

Most of the chip forms are approximately triangular. As the feed increases at any depth of cut, the curved boundary on the top of the chip becomes shorter and the feed portion larger. Finally, the tool only cuts a circular groove. As that condition is approached, the chip shape is more nearly trapezoidal. An approximately trapezoidal form is made when the depth of cut approaches or exceeds the tool nose radius. Then, the straight side of the tool adds a contribution. This is shown in Figure 16. Those deeper cuts will be analyzed in a later report. A final way trapezoidal chip cross sections are formed is by deforming or

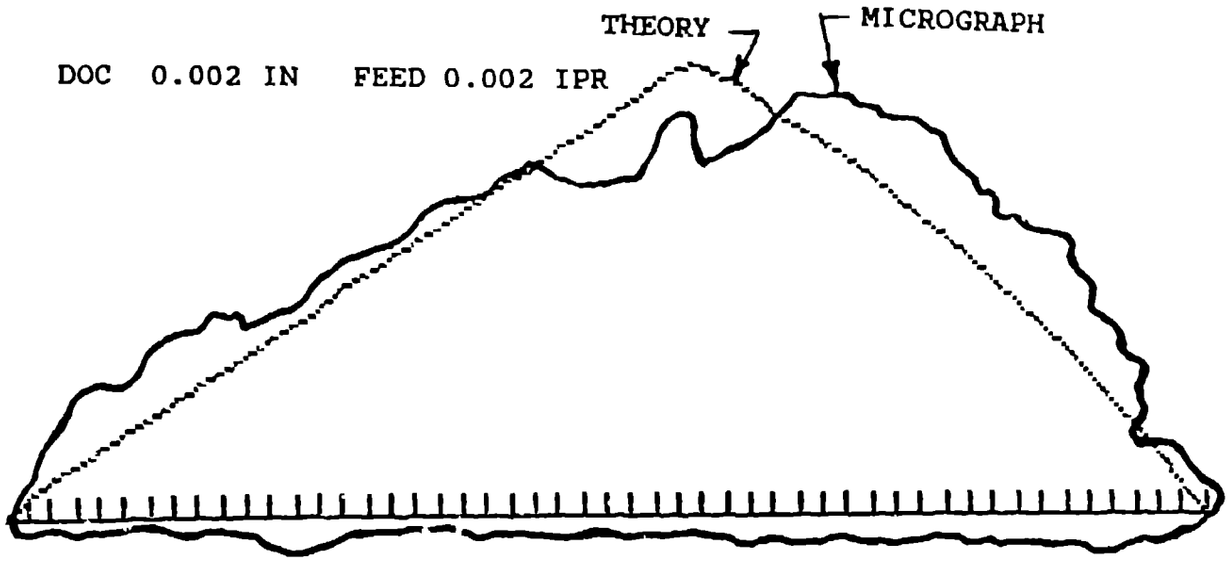

Figure 11 Very Light Cut (0.002 in DOC)

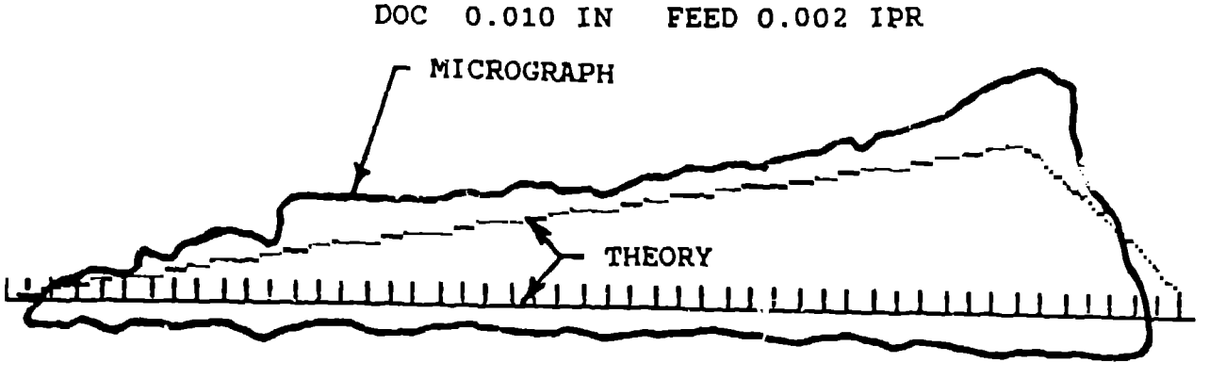

Figure 12 Light Cut (0.010 in DOC)

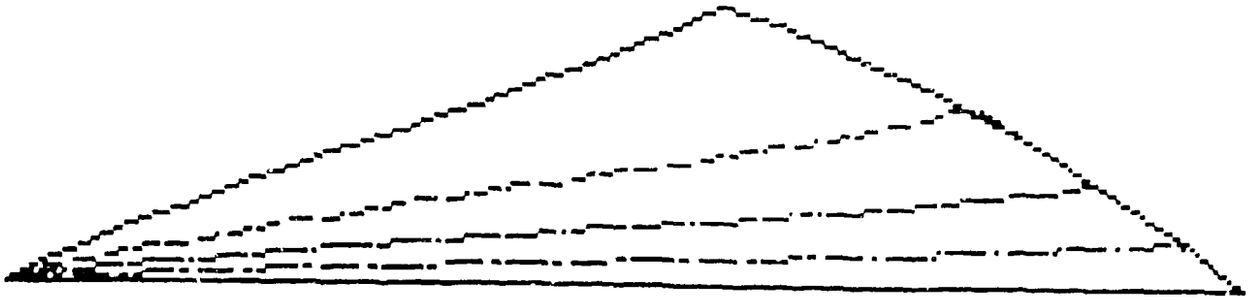

F = 2/3 F = 1/3 F = 1/6 F = 2/30

Constant Cut Depth 2/3

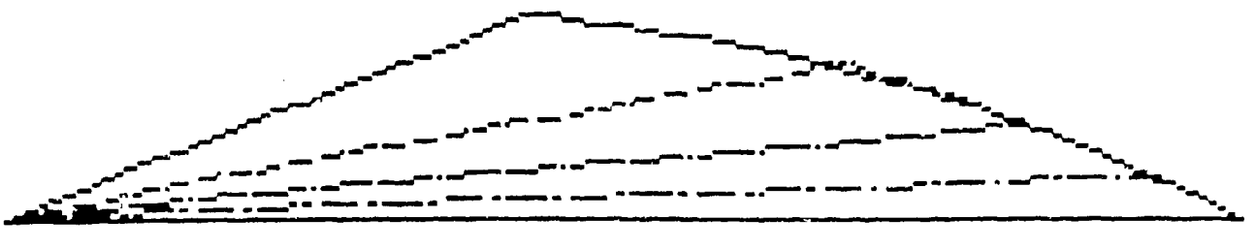

F = 2/3 F = 1/3 F = 1/6 F = 2/30

Constant Cut Depth 1/3

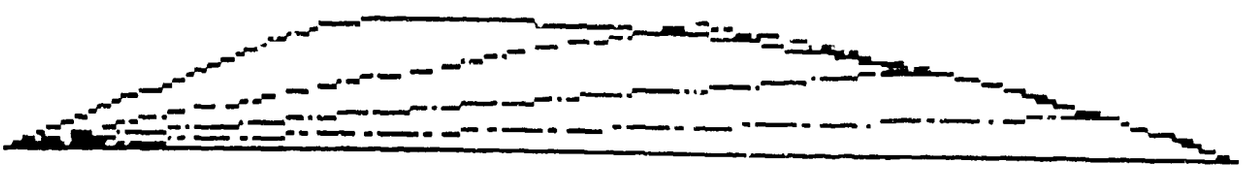

F = 2/3 F = 1/3 F = 1/6 F = 2/30

Constant Cut Depth 1/6

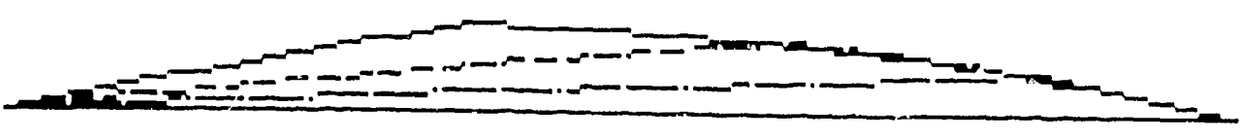

F = 2/3 F = 1/3 F = 1/6 F = 2/30

Constant Cut Depth 2/30

Figure 13 Chip Cross Section Variation with Feed

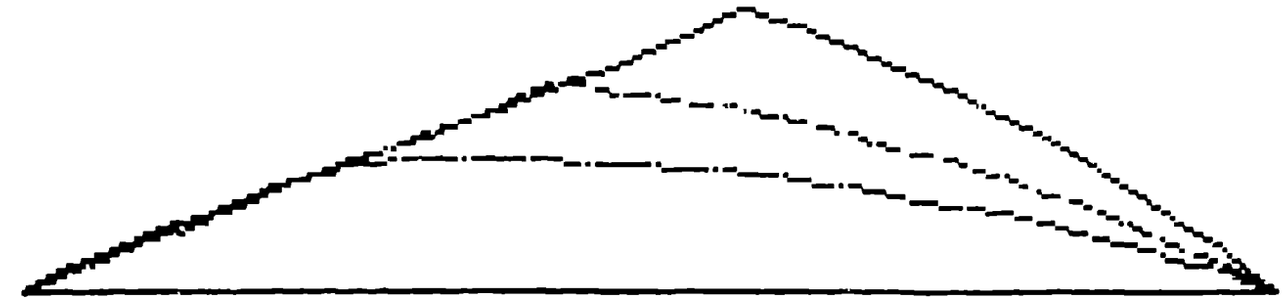

DOC/N RAD = 2/3 DOC/N RAD = 1/3 DOC/N RAD = 1/6 DOC/N RAD = 2/30

Constant Feed 2/3

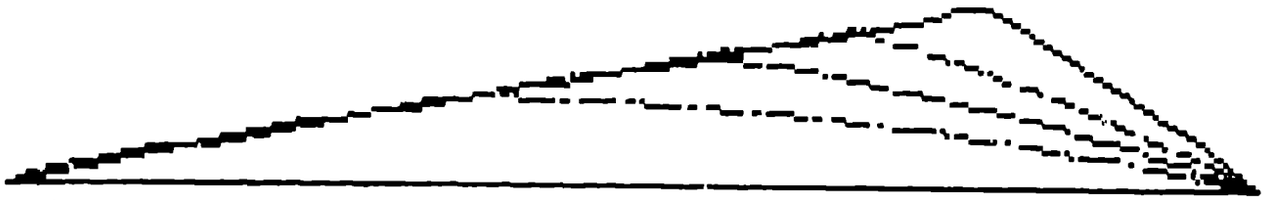

DOC/N RAD = 2/3 DOC/N RAD = 1/3 DOC/N RAD = 1/6 DOC/N RAD = 2/30

Constant Feed 1/3

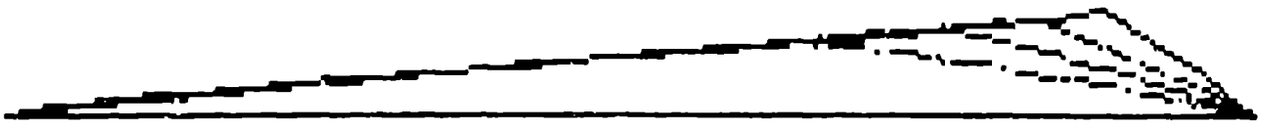

DOC/N RAD = 2/3 DOC/N RAD = 1/3 DOC/N RAD = 1/6 DOC/N RAD = 2/30

Constant Feed 1/6

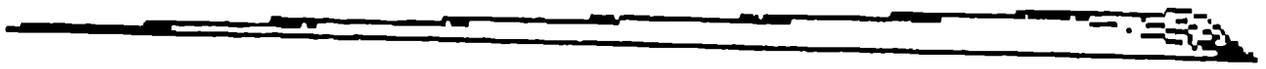

DOC/N RAD = 2/3 DOC/N RAD = 1/3 DOC/N RAD = 1/6 DOC/N RAD = 2/30

Constant Feed 2/30

Figure 14 Chip Cross Section Variation with Depth of Cut

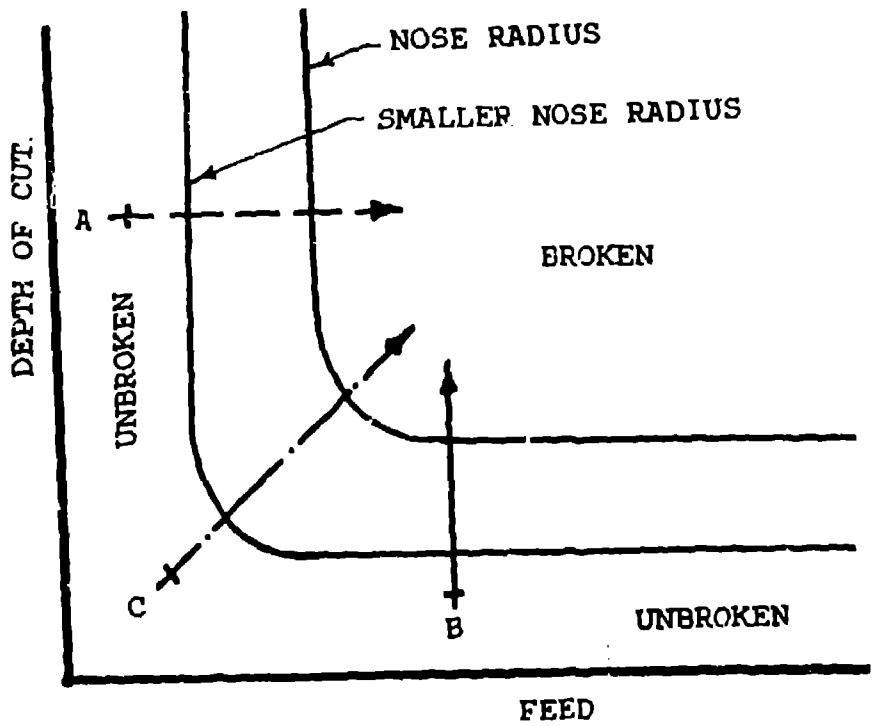

Figure 15 Typical Chip Breaking Diagram

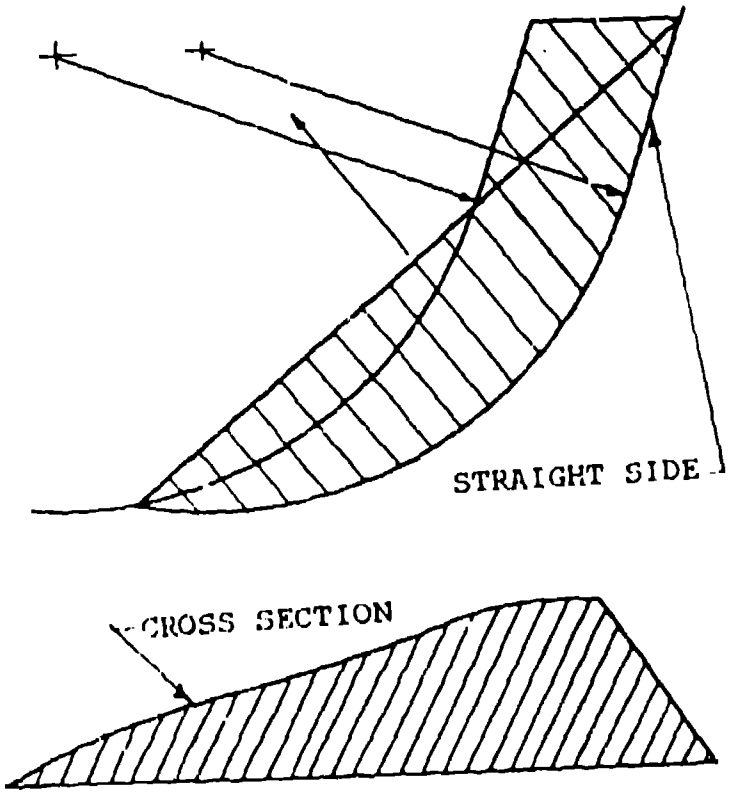

Figure 16 Cuts Deeper than the Nose Radius

breaking off one of the vertices of a triangular shaped chip. A summary of the changes in chip thickness and vertex position will be given in the next section where it will be used to show the change in stress.

Since the chip thickness relative to the uncut chip thickness depends on the machining conditions and the coefficient of friction, the relation of chip thickness to shear angle is shown in Figure 17. Changes in shear angle depend strongly on the coefficient of friction at the tool-chip interface. Only the chip thickness is changed by the shear angle, not the position of the vertex. Figure 18 depicts the way the shear angle alters the chip cross section. The tool's chip breaking grooves or obstruction design can change the shear angle. Therefore, the actual chip thickness depends on the tool design. Conversely, a study of the chip cross section permits evaluation of the shear angle.

ANALYSIS OF THE STRESSES AT EACH CROSS SECTION VERTEX

Notice that all of the cross sections, especially where there was no spring back were approximately triangles. The centroid of a triangle is located 1/3 the distance between the midpoint of an opposite side and its associated vertex. Visual observation of Figures 5-12 shows that in most cases the top vertex is closest to the centroid. Thus, bending the chip in a direction normal to the tool rake face (vertical on the Figures shown) would produce lower stresses at that vertex for the same bending displacement than a similar displacement might produce at the other vertices. However, the vertex in the normal chip flow direction could be more vulnerable to fracture because of stress concentrations and work hardening. The relation between the chip cross section and the stress produced at the vertices assists in a test of the relative ease of breaking. The variations in the shape of the cross section are then related to the cutting variables. Thus,the relation between the ease of breaking and changes in the cutting variables of cut depth, feed, and tool nose radius can be examined. Appendix II shows the derivation of the chip cross sectional properties for stress evaluation.

COMPARISON OF VERTEX STRESSES

The stresses will be evaluated to compare the most advantageous direction for applying chip breaking loads. It will be assumed that the chip is a cantilever beam of triangular cross section. The chip breaker will be assumed to apply a displacement U_b by virtue of its height above the tool face. Figure 19 shows the cantilever and its relation to the tool and chip breaker. The obstruction type chip breaker was chosen for convenience, but the same analysis would apply to other types of breaking designs. Also, for the present, the applied load will be assumed to pass through the shear center of the chip, producing only bending. Torsional stresses can be calculated using the equations in Appendix II. Then when the load does not pass through the shear center, estimates can be made by combining flexural and torsional stresses. While the vertex at the chip thickness would normally be in compression by the chip breaker induced loads, the base of the triangle would experience half as much stress in tension by those loads. The upper surface would be in tension in the reverse bending described by Nakayama[7], and that is the advantage of trying to break chips in that manner. However, the reverse bending would have a longer cantilever beam length and require a proportionately larger displacement to

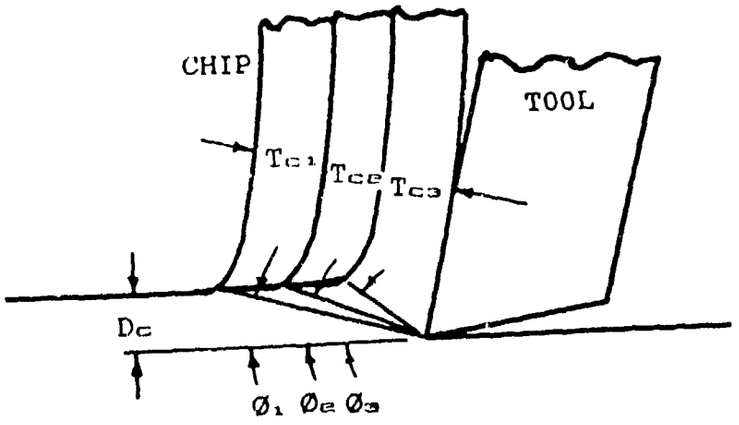

Figure 17 Relation of Chip Thickness and Shear Angle

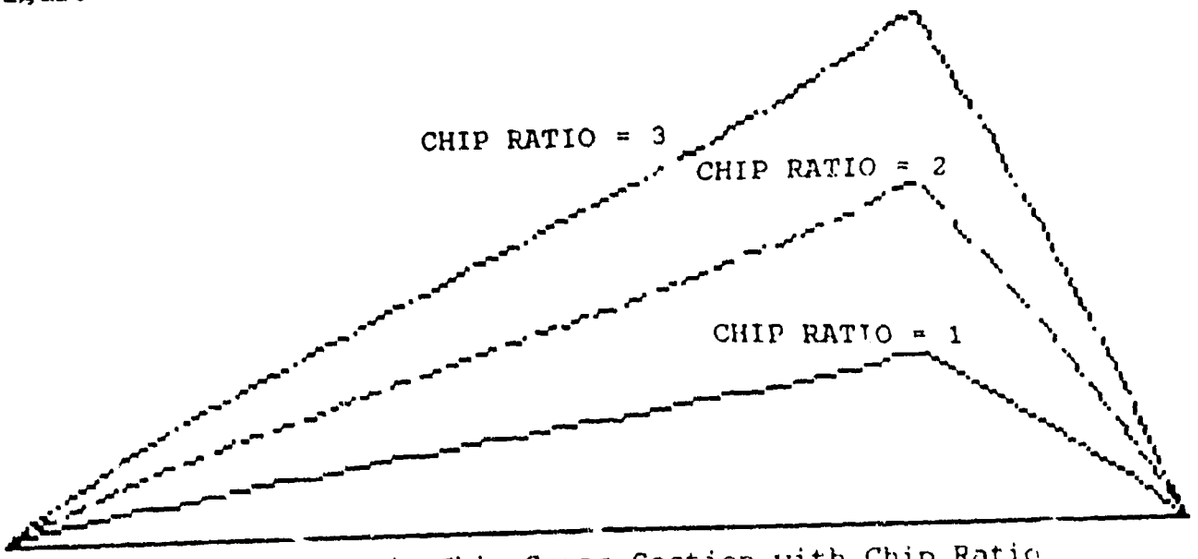

Figure 18 Changes in Chip Cross Section with Chip Ratio

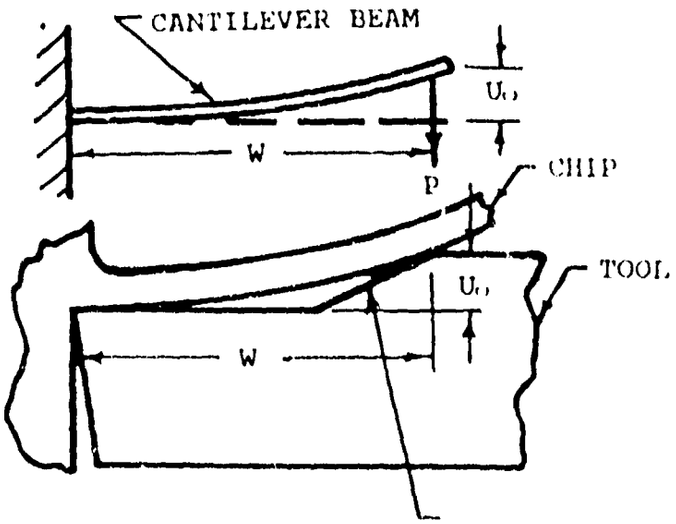

Figure 19 Chip Breaking or Normal Curling Displacements

achieve the same stress value.

Noting that the deflection of a cantilever beam, is given by:

$$U_b = PW^3/3EI = MW^2/3EI$$

where W is the cantilever length between the tool tip and the top of the chip breaker, E is the elastic modulus, and I is the moment of inertia. P is the load and M = PW is the applied moment. Examination shows that when the deflection U_b is constant, the moment is:

$M = K_1 U_b I$, where K_1 is a constant containing the elastic modulus and chip breaker setback terms. The vertex stress per unit breaker height is:

$$S_{1B}/U_b = K_1 c_{1v}$$

where c_{1v} is the projected vertical distance between the centroid and the thickness vertex. All other terms are constants. Similar relations apply to bending in the transverse direction (parallel to the rake face).

Using the information on Figure 13 and plotting the thickness at the vertex results in Figure 20. The individual curves represent the different depths of cut. Note that most of the curves reach a maximum. If a horizontal line were selected on Figure 20, that would represent a constant stress per unit displacement of the cantilever chip beam. One such curve should represent the failure stress level for some material. A series of curves should represent several failure stress levels.

Thus Figure 21 represents lines of failure or regions of breaking chips by plotting the constant thickness lines from Figure 20. Recalling the composite of numerous experimental efforts in Figure 15, the similarity can be seen. Thus, the theory gives a physical basis for a history of observations.

A large family of curves could be produced on Figure 21 each for a different chip thickness or failure stress level. Figure 20 assumed the undeformed chip thickness was the same as the deformed thickness. For a tool with a zero or neutral rake angle that would correspond to a shear angle of 45°. Figures 17 and 18 showed the variation of chip thickness with shear angle. Thus, a tool producing a smaller shear angle would make a thicker more easily broken chip. It is possible that the variations in the experimentally determined diagrams in the literature are primarily a result of variations in the shear angle produced.

Since in many of the chips shown in Figures 5-12 and the cross sections calculated in Figures 13-14 the distances to other vertices are larger than from the centroid to the thickness vertex, it should be advantageous to try to bend the chips in the transverse direction. Also the more distant vertices would have larger stress under torsional loading. Ioffe[12] produced a roller type chip breaker to produce a side or transverse displacement of the chip. The transverse load plus torsion is the type of loading produced by the chip weight and by coolant loading on straight chips, small snarls, and short helical forms. It has been puzzling to know why a helical form would regularly break and form short helices. All that is needed to complete that failure mode is to derive the loading in terms of weight and viscous

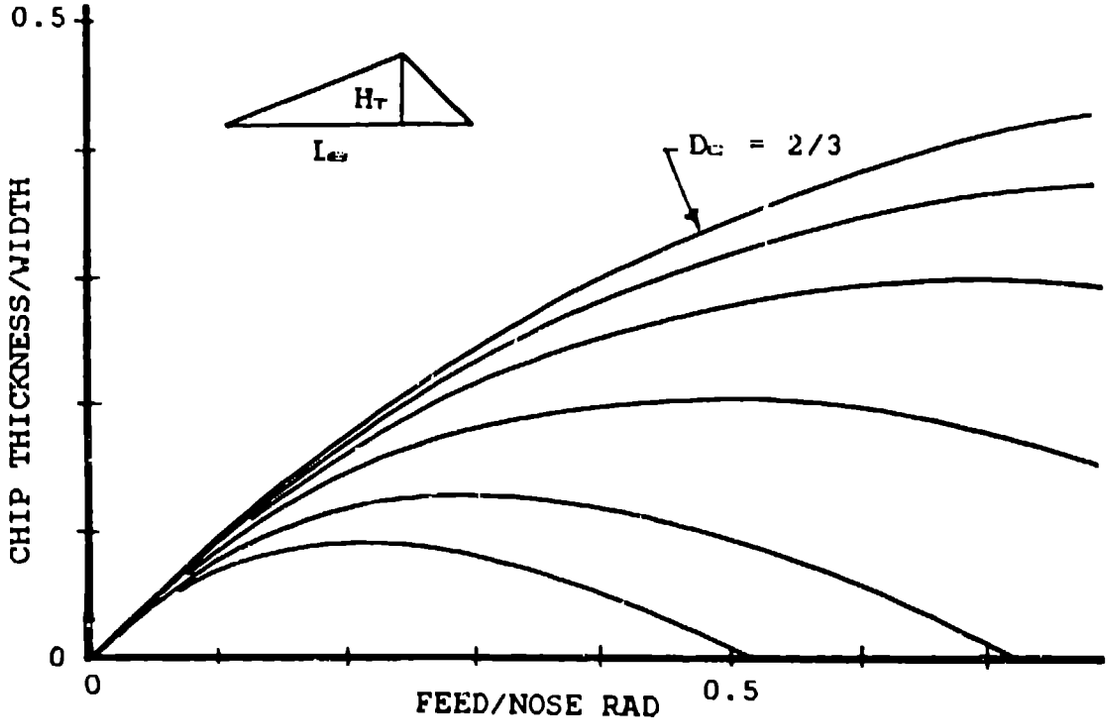

Figure 20 Relation of Chip Thickness to Cutting Parameters

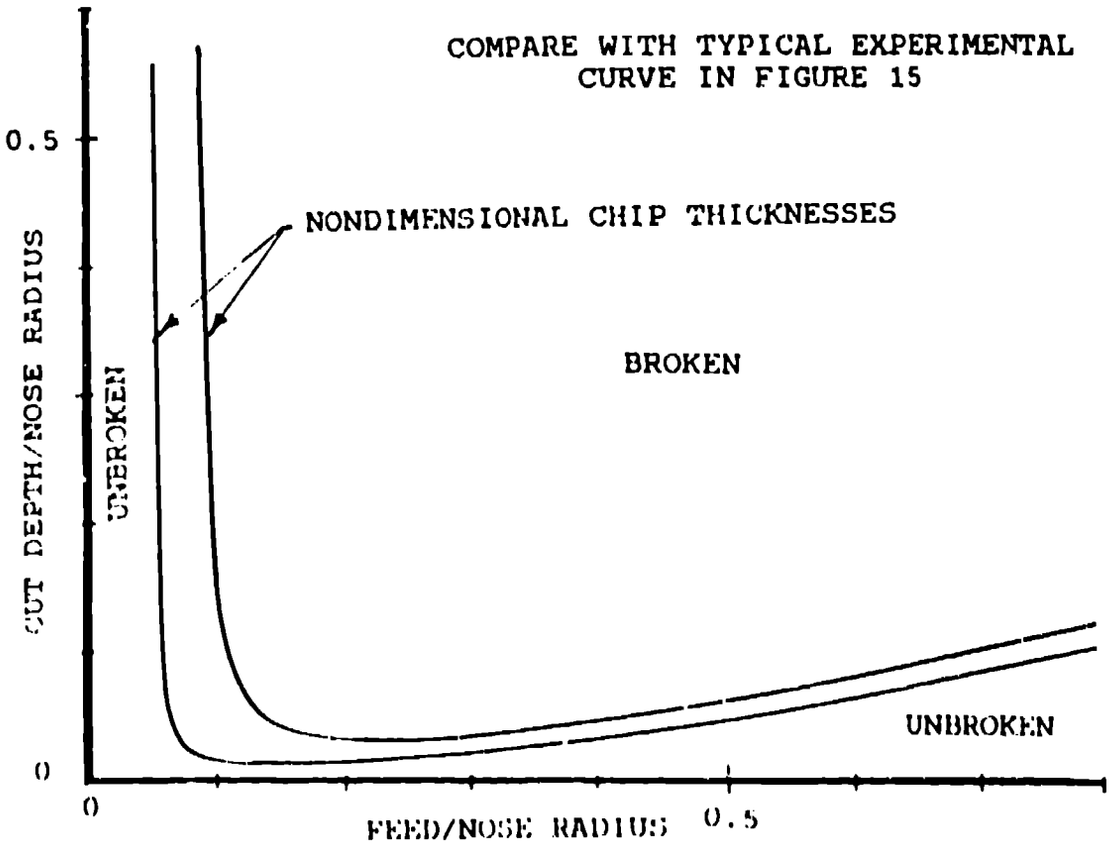

Figure 21 Theoretical Chip Breaking Diagram

drag on the helix, then combine it with the previous stress analysis. A plot similar to Figure 20 could be made for the vertex position of the vertex opposite the rake face. Then a strategy of feeds and cut depths could be based on a constant vertex position so that the shear center did not shift, making one breaker design more generally applicable.

LOADS ON HELICAL CHIPS

When a straight, helical, or snarled shaped chip is formed, there are loads produced by a combination of the chip weight and the coolant applied. The coolant can be applied from any direction all the way from vertical to horizontal on either side of the tool. Usually, the nozzle position is set by the operator. Also, the coolant jet can be pulsed to accomplish control of the length of the helix.

The loads produced by the flowing coolant are viscous drag forces. These forces are related to the coolant velocity, the drag coefficient, and the chip area exposed to the flow. A straight chip presents only a small area in the region of the chip flow. A vacuum system or a gas jet has been used to break and remove fine straight chips in diamond turning. Presented area for helical or coiled chip forms can be derived using the chip curl results reported as a basis[3,10,11]. The area for snarled chip forms can only be estimated since the snarl is seldom a regular geometry. It can be calculated as a sphere and the percent of the area occupied by the chip solids estimated to get the area of loading. In many cases, these loads produce both torsion and transverse bending on the chip so that the vertex farthest from the centroid of the cross section receives the largest stress.

The weight of the chip form results from calculating the volume of the chip material in the unbroken form. For example, a short helix weight would be the length of the spiral up to the breaking length multiplied by the cross section area and the material density. In both the coolant drag loading and the weight, the force is assumed concentrated at the mid length of the chip form. A detailed derivation is given in Appendix III.

The coolant and weight loads have not been tested yet, but several cases can be estimated. The analysis serves to specify the variables needed to investigate producing short helix forms of broken chips. A basis is also given to study the best positioning and pulse frequencies for coolant streams. Note that helices produced by sideways curling of the chip (See Nakayama[3]) would require replacing the chip width, with the chip thickness in the area calculation and perhaps changing the pitch of the helix. Generally, these chip forms would be harder to break since the presented area is smaller for the same pitch.

CONCLUSIONS

Abbatiello[10] found that in the case of hydraulically assisted chip breaking, the chips were about 10 times easier to break in the transverse direction. That is, an order of magnitude lower jet pressure broke chips in the transverse or sideways direction compared with breaking in a normal direction. A complete range of spherical angles for jet orientation were evaluated, and those results are applicable to the coolant flow considered.

Ioffe[18] found that a roller on top of the tool to deflect the chip to one side (transverse loading) was very effective in breaking chips. That agrees with the observations based on the chip cross section.

Combined coolant delivery and chip breaker designs to make use of the modes of loading most likely to break chips may be considered. Unfortunately, mechanical breakers are difficult to design for transverse chip loading. Torsion also appears more effective in contributing to chip breaking. Perhaps we need a new twist for good chip breaking.

Strategies to break chips when in an unbroken regime cannot merely rely on changing a single cutting variable but must account for all the chip shape changes and the relation to the action of the chip breaker. Calculating the shear center and using a load at the high point of the initially curved chip bottom may permit a prediction of chip curl.

ACKNOWLEDGMENT

This work was done with the assistance and encouragement of the United States Department of Energy, Albuquerque Operations Office, and support was received through contract no. 9-XFH-55265-1 with the Los Alamos National Laboratories. The effort is part of the Department of Energy concern for a safe working environment and for a healthy community through waste minimization without compromise in quality. The support and encouragement are appreciated and acknowledged.

BIBLIOGRAPHY

1. Burnham, M.W., & Abbatiello, L.A. "Chip Breaking for an Automated Accurate Turning System", 4th Biennial International Machine Tool Technology Conference, NMTBA, 1988.

2. Colwell, L.V., "Predicting the Angle of Chip Flow for Single Point Cutting Tools", ASME Trans, 76, (2), pp 199-204, 1954

3. Nakayama, K.,"Chip Control in Metal Cutting", BJSPE, 18, (2), pp 97-103, 1984

4. Kane, G.E., "The Effect of Tool Geometry on Chip Breaking", Soc. Mfg. Engrs Paper # MR71-923, 1971

5. Kane, G.E., "An Approach to the Breaking of Chips", ASM Int'l pp 29-37, Feb 1987

6. Jiang, C.Y., Zhang, Y.Z., & Chi, Z.J., "Experimental Research of the Chip Flow Direction and its Application to the Chip Control", Annals of CIRP, 33, (1), pp 81-84, 1984

7. Nakayama, K., & Arai, M., "On the Storage of Data on Metal Cutting", Annals of CIRP, 25, (1), pp13-18, 1976

8. Kon-ichiro Oh uchi & Kazuhiko Asano, "Chip Breaker, with the Chip Flow Direction Taken into Consideration", R&D Kobe Steel Engrng Reports, 46, (4) pp 1-11, 1988

9. Nakayama, K., & Arai, M., "The Breakability of Chip in Metal Cutting", Int'l Conf on Mfg Engrng, Melbourne, AUS, pp 6-10, 1980

10. Spaans, C., & Van Geel, P.F.H.J., "Break Mechanisms in Cutting with a Chipbreaker", Annals of CIRP, 18, pp 87-92, 1970

11. Kluft, W., Konig, W., Van Luttervelt, C.A., Nakayama, A, & Pekelharing, A.J., Present Knowledge of Chip Control", Annals of CIRP, 28, (2), pp 441-455, 1979

12. Ioffe, N.M., "Dynamic Chip Breaker", Stanki i Instrument, (11), pp 18-20, 1949

APPENDIX I. Derivation of the Chip Boundary Relations

Consider a tool tip which is a portion of a circle representing a tool with nose radius r_n moving into the workpiece material by a feed f, each revolution at a depth d_c below the uncut surface.

Assume for the moment that there is no spring back of the chip after it is formed, and that the shear angle is the same for each chip element at the tool tip circle. The effect of spring back will be shown later, and the validity of the shear angle assumption will be shown experimentally. If the shear angle is the same for all elements, what would be the shear plane in orthogonal cutting is a shear surface curved almost the same as the tool nose. It is approximately circular because the shear angle imposes a small ellipticity, since the shear plane is not identical to the normal to the tool rake face. Notice that the curvature to the shear surface requires a locus of the intersection of the shear surface and the uncut surface as shown in the top surface (the dashed line) of Figure 1. This intersection or chip initiation contour, then must define the top side of the chip, away from the rake face.

Each element at the tool tip has a slightly different effective uncut chip thickness from the adjacent element; therefore the length of the associated shear plane depends on location along the tool tip. This implies a variation of force distribution around the tool tip. The shading in Figure 1 shows the resultant shear surface. It can be seen that at the ends of the cutting edge chord (CEC) the undeformed chip thickness is zero while at the midpoint of the chord, the thickness of is maximum. Figures 2 & 3 show the uncut chip cross section. The strain deformation change between an element on the tool tip and an adjacent element is represented by the shaded segment of a circle. So while the length of the shear surface varies, proportional to the width of the uncut chip normal to the CEC, the relative strain displacement varies according to the width of the circular segment. This may be why the CEC model has worked so well in experimental tests. It represents the termination of relative shear strain and establishes the base of the chip cross section. Many papers[4,5,6] have reported excellent agreement with Colwell's CEC model by observations of the chip flow direction as normal to the CEC.

Using the notation in Figure 2, it is convenient to change the position of the x and y axes to be located parallel and normal to the cutting edge chord as in Figure 22. This requires rotating the body by

$(\theta_o+\theta_i)/2$ where θ_o and θ_i are the angles to the two ends of the CEC in Figure 2. First normalizing x, y, d_c, and f:

Let $X = x/r_n$, $Y = y/r_n$, $D = d_c/r_n$, and $F = f/r_n$

$$\cos(\theta_o) = 1-D \qquad [1]$$

$$\sin(\theta_i) = F/2 \qquad [2]$$

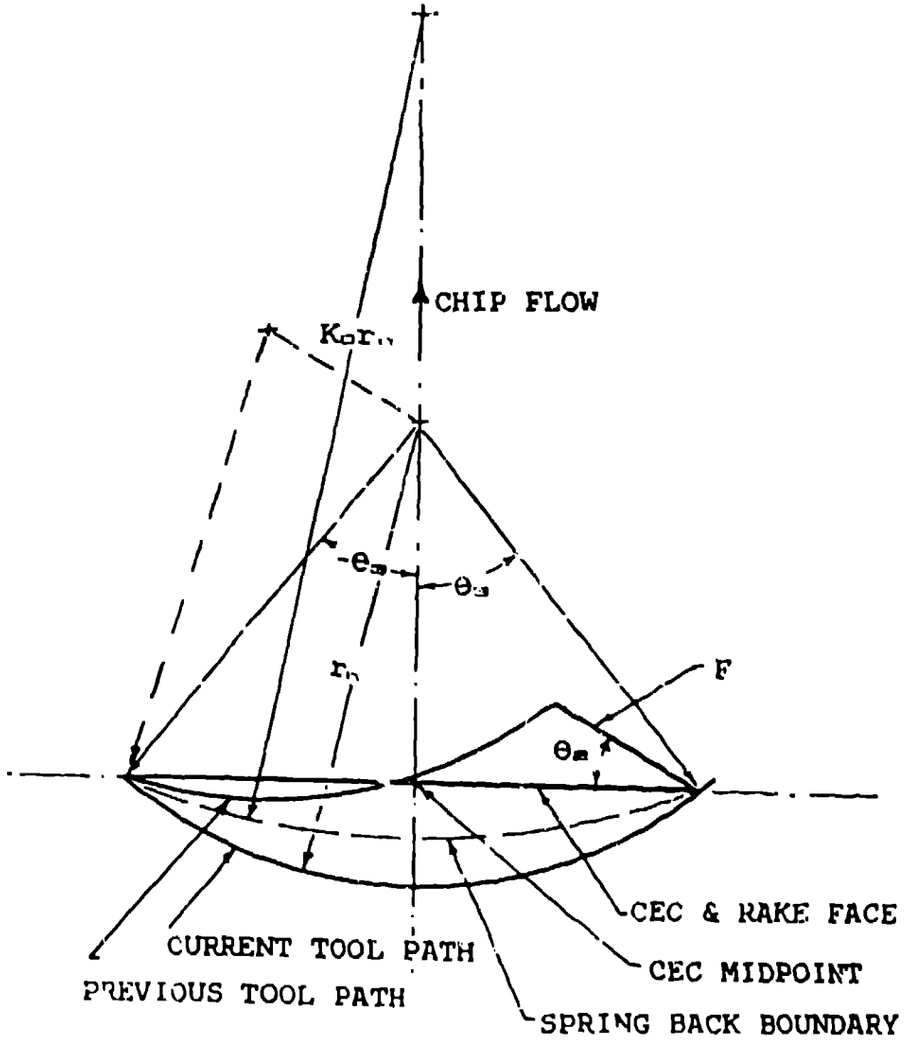

Figure 22 Chip Analysis Orientation

The angle between the original uncut part surface and the cutting edge chord is obtained from the inverse of:

$$\tan(\theta_m) = [D - 1 + \cos(\theta_i)]/[\sin(\theta_o)+F/2] \qquad [3]$$

$$\theta_s = (\theta_o+\theta_i)/2 \qquad [4]$$

The left portion of the upper uncut chip boundary in Figure 22 is from $X = -l_c/2$ to $\sin(\theta_i - F\cos(\theta_m)$:

The normalized chord length is;

$$L_c = 2\,\mathrm{Sin}(\theta_3)$$

Letting, $\mathrm{Sin}(\gamma) = X$
and, $\mathrm{Sin}(\delta) = [X + F\,\mathrm{Cos}(\theta_2)]$

Then the left portion of the undeformed chip thickness is defined by:

$$Y_U = \mathrm{Cos}(\gamma) + F\,\mathrm{Cos}(\theta_2) - \mathrm{Cos}(\delta) \qquad [5]$$

And when the limits on X are: $X = \mathrm{Sin}(\theta_3) - F\mathrm{Cos}(\theta_2)$ to $L_c/2$, the uncut or right portion of the upper boundary is:

$$Y_U = \mathrm{Cos}(\gamma) + \mathrm{Tan}(\theta_2)[\mathrm{Sin}(\theta_3) - X] - \mathrm{Cos}(\delta) \qquad [6]$$

The lower boundary which also represents the amount of relative strain between elements along the work surface in contact with the tool nose is defined by:

$$Y_L = [1 - \mathrm{Cos}(\gamma)] \qquad [7]$$

Since the chip forming process forces the lower boundary up to the cutting edge chord, the value of Y_L in equation[7] is included in equations [5] & [6]. These Y values represent the uncut chip cross section, and when multiplied by the chip ratio (the ratio of the deformed chip thickness to the undeformed thickness), produces the boundaries of the cut chip. The lower boundary is a straight line if there is no relaxation or springback. The chip ratio it may be recalled is:

$$p = \mathrm{Cos}(\phi - \alpha)/\mathrm{Sin}(\phi) \qquad [8]$$

Where ϕ is the shear angle and α is the rake angle.

Therefore, if Y_c represents the Y values transformed to the plane of the chip thickness, then:

$$Y_c = p\,Y \qquad [9]$$

Where Y is defined by equations [5] & [6]

The springback is represented by a larger radius on the uncut chip diagram in Figure 22. Since $Y = y/r_n$, if there is a larger radius curve to be subtracted from the boundary equations [5,6], it would be defined by:

Let k_o be a factor increasing the radius r_n of the current tool path or lower boundary with a center located on the X axis. Then,

$$\mathrm{Sin}(\gamma_n) = x/r_n k_o = X/k_o \qquad [10]$$

at the chord end where the tool paths intersect,

$$\mathrm{Sin}(\gamma_o) = L_c/(2k_o)$$

and the springback displacement is:

$$Y_{e} = [\mathrm{Cos}(\gamma_{e}) - \mathrm{Cos}(\gamma_{o})] \quad [11]$$

The top contour representing the chip cross section is then:

$$Y_{ce} = \rho[\ Y - Y_{e}\ ] \quad [12]$$

and the bottom cross sectional chip boundary is:

$$Y_{eo} = \rho\ Y_{e} \quad [13]$$

If the workpiece is a strain hardening material, and the chip is cooled rapidly enough to prevent annealing of the chip, the value of Y_e when compared with the displacement Y_L (equation [7]) can be correlated to the amount of strain hardening experienced as illustrated in Figure 4. Although a linear plasticity model is assumed, it can be seen that as the total displacement increases and the slope of the plastic portion of the curve increases, the increment of elastic relaxation increases on unloading. Thus, in the case of the chip springback, the elements at the ends of the cutting edge chord would have no relaxation strain or springback while those near the center would have the maximum displacement.

APPENDIX II Derivation of Cross Sectional Properties

Before the chip is deformed from the curved shape to the almost triangular shape in the chip formation process, the curved chip area oriented to the cross section of the chip is:

$$A_{e} = [F\ (\mathrm{Cos}\ \theta_{1} - \mathrm{Cos}\ \theta_{o}) + \theta_{1} - \mathrm{Sin}(2\theta_{1})/2\ ]\ \rho \quad [14]$$

This is the exact theoretical area of the chip. If the chip ratio is 1 and the rake angle of the tool is zero, this is the area of the uncut chip in the workpiece, normal to the tool path. A very good approximation can be obtained by multiplying the cut depth by the feed. This slightly over-estimates the area of the chip.

Using the true area, assuming that the top arc is lengthened and the bottom (current tool edge) arc is shortened by the same amount to produce a triangle of the same area, the amount by which the arcs are lengthened and shortened is:

$$E_{1} = \theta_{1} - [(F/2)^{n} - (A_{e})^{n}/[(\theta_{1})^{n} - (F/2)^{n}]^{n}]^{1/n} \quad [15]$$

The length of the bottom (current tool edge arc) triangle side, when normalized (divided by the tool nose radius) is:

$$L_{e} = \theta_{o} + \theta_{1} \cdot E_{o} \quad [16]$$

Then the triangle height is:

$$H_{T} = A_{e}/(2\ L_{e}) \quad [17]$$

and the proportion of L_e from the vertex at the tool tip and the workpiece surface (intersection of F and L_e) is:

$$S_{T} = [\ F^{n} - H_{e}^{n}\ ]^{1/n} \quad [18]$$

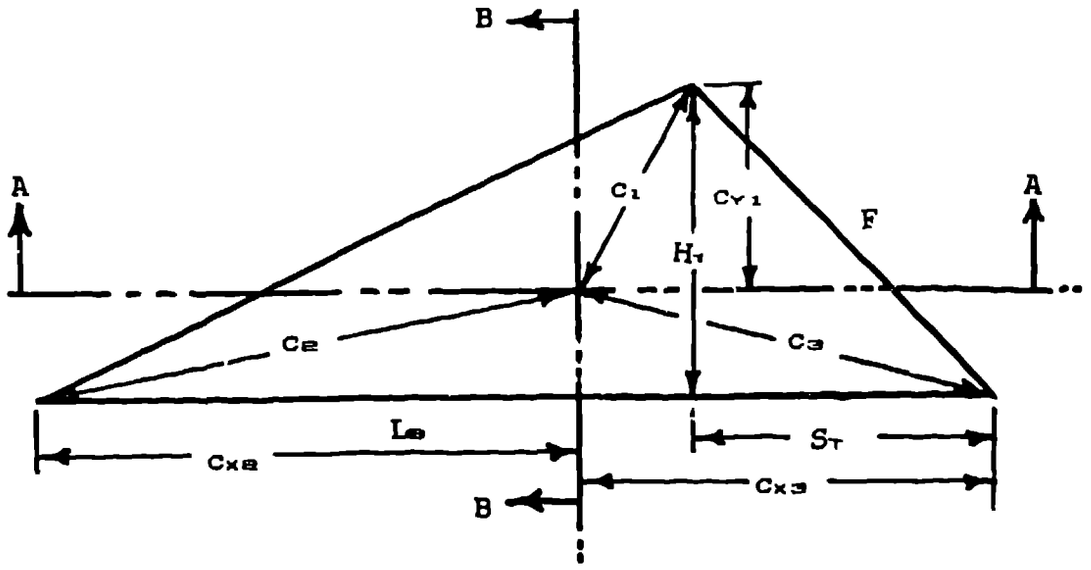

Figure 23 Triangle Approximation

Using the notation in Figure 23, the moment of inertia at the centroid and parallel to the X axis (for normal bending in a direction normal to the rake face of the tool) is:

$$I_{BB} = L_B (H_T)^3/18 \qquad [19]$$

From the triangle geometry, the angles at vertices 3 and 2 are obtained from:

$$\mathrm{Sin}(\psi_3) = H_T/F$$

$$\mathrm{Tan}(\psi_2) = H_T/[(1-S_T) L_B]$$

$$\text{Let } I_0 = \{[(1-S_T)\mathrm{Cos}\ \psi_2]^2+[F\mathrm{Cos}\ \psi_3]^2\}/6$$

Then the moment of inertia at the centroid and normal to the base L_B (for transverse bending) is:

$$I_{BB} = A_B\{I_0+[(2/3)L_B(1-[1-S_T]\mathrm{Cos}\ \psi_2)-F\mathrm{Cos}\ \psi_3]^2\} \qquad [20]$$

The projection on the Y axis of the distance from the centroid to vertex 1 is:

$$c_{1V} = (2/3)\ H_T \qquad [21]$$

and on the X axis of the centroid to Vertex 3 distance:

$$c_{3X} = L_B(1 + S_T)/3 \qquad [22]$$

and on the X axis of the centroid to Vertex 2 distance:

$$c_{2X} = L_B - c_{3X} \qquad [23]$$

The corresponding distances from the centroid to the three

vertices is:

$$C_1 = (2/3)[L_{AB}^e(0.5-S_T)^e+H_T^e]^{1/e} \quad [24]$$

$$C_3 = [c_{3x}^e + (H_T/3)^e]^{1/e} \quad [25]$$

$$C_2 = [c_{2x}^e + (H_T/3)^e]^{1/e} \quad [26]$$

Now the bending stresses at the vertices can be calculated. Vertex 1 will be subject to stress by bending in the normal direction while the other two vertices will be placed under maximum stress by transverse bending. In each case, the stress will be normalized by dividing by the moment.

$$S_1/M = c_{1y}/I_{AA} \quad [27]$$

$$S_2/M = c_{2x}/I_{BB} \quad [28]$$

$$S_3/M = c_{3x}/I_{BB} \quad [29]$$

Likewise the torsional stress at each vertex for a torque T applied to chip is:

$$S_{s1} = C_1/(I_{AA}+I_{BB}) \quad [30]$$

$$S_{s2} = C_2/(I_{AA}+I_{BB}) \quad [31]$$

$$S_{s3} = C_3/(I_{AA}+I_{BB}) \quad [32]$$

For a chip in the form of a cantilever beam built in near the chip root and bent in a direction normal to and away from the rake face, the deflection by the chip breaker U_c at a distance W from the fixed end is

$$U_c = P W^3/3EI = M W^2/3EI = M/K_1 I$$

where P is the force, E is the elastic modulus, and I is the moment of inertia, I_{AA} or I_{BB} for normal and transverse bending directions respectively. Using these in equations[27-29] produces equations relating the bending stress directly to the c distances. A similar relation relates the torsional stresses directly to the distance between the centroid and the vertex of interest for a specified angular displacement about the chip axis.

APPENDIX III Loads on the Chip

When the cutting speed V_c is reduced to inches/second and is divided by the chip ratio to represent chip velocity, if the chip forms a helix of pitch p_c and has a chip width of b, the length of chip per second is:

$$l_c = V_c b^2 p_c/(10^7 r_c p) \quad [36]$$

Then the surface area of the chip per second times the component of coolant jet velocity V_j and the drag coefficient K_c produce a jet force normal to the axis of the helix. That is:

$$F_j = V_j V^2_c K_c b^2 p_c/(5^7 p) \quad [37]$$

The force produced by the weight of the helix depends on the angle of the helix axis and the weight of the helix assumed to act at half the length. Thus:

$$F_w = V_w b^E p_c w_c \mathrm{Cos}(\beta_j)/(10^{\pi}\ p) \qquad [38]$$

And the combined force normal to the helix axis is:

$$F_c = V_w b^E p_c [K_E V_j \mathrm{Cos}(\alpha_j) + (w_c/2)\mathrm{Cos}(\beta_j)]/(5^{\pi}\ p) \qquad [39]$$

And the torque at the chip root is:

$$T_c = F_c l_c \qquad [40]$$

If the helix is not horizontal and the jet is not vertical to the helix axis, then there is a transverse bending force at the chip root which can be calculated by replacing $\mathrm{Cos}(\alpha_j)$ and $\mathrm{Cos}(\beta_j)$ with $\mathrm{Sin}(\alpha_j)$ and $\mathrm{Sin}(\beta_j)$ in equation [39]. Attention must be given to the signs of the force components of the coolant and the chip since they can be in opposite directions depending on the orientation of the helix and the jet.